

# Optics and Detector Modifications for TRINAT's Time-Reversal Experiment

Michelle Khoo

(UBC Science Co-op 2021S, Part-time 2021F-2022W)

Supervisor: John Behr, TRINAT

# Contents

<b>1</b>	<b>Background</b>	<b>2</b>
1.1	Theory . . . . .	2
1.2	Gamma Detection . . . . .	2
<b>2</b>	<b>355nm Laser and Fiber Coupling</b>	<b>3</b>
2.1	Beam Size/Shape . . . . .	4
2.2	Fiber . . . . .	4
2.3	Optical Assembly . . . . .	5
2.4	Procedure . . . . .	7
2.5	Results . . . . .	8
<b>3</b>	<b>Gamma Detector</b>	<b>9</b>
3.1	Bias Voltage Optimization . . . . .	9
3.2	Wrapping Sensitivity . . . . .	9
3.3	Timing and Energy Signal Generation . . . . .	11
3.4	Results . . . . .	12
<b>4</b>	<b>References</b>	<b>13</b>

# 1 Background

## 1.1 Theory

TRIUMF's Neutral Atom Trap (TRINAT) is searching for time-reversal symmetry violating interactions in the beta decay products of trapped atoms. The experiment uses a magneto-optical trap (MOT) to confine atoms, and then optically pumps the trapped atom with a 770 nm beam (see Figure 1a). The atom's polarization is probed by photoionizing  $\sim 1\%$  of the population with a 355nm beam (see Figure 1b).

It is known that the scalar triple product of momenta

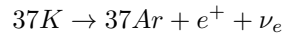
$$p_1 \cdot p_2 \times p_3$$

always flips sign with time. Therefore, a time-reversal violating interaction would produce a non-zero average scalar. However, if a three-momentum state is probed, this scalar will always average to zero by momentum conservation. To resolve this, we search for beta-neutrino-gamma coincidences

$$p_\beta \cdot p_\nu \times p_\gamma$$

for the radiative beta decay branch, which is a four-momentum state ( $p_{recoil}$ ,  $p_\beta$ ,  $p_\nu$ , and  $p_\gamma$ ).

Beta-plus decay of  $^{37}\text{K}$



is used for the time-reversal experiment. Note that for test runs, beta-minus decay of  $^{45}\text{K}$



is used as its gamma ray spectrum has two clear peaks at 1706 keV and at 2354 keV/2349 keV. Having two peaks is useful for determining the offset and slope (ie. gain) when mapping gamma energy to spectrum channel of the detector's output.

## 1.2 Gamma Detection

The decay products are detected by a GAGG (Gadolinium Aluminium Gallium Garnet) scintillator with passively summed SiPM readout. GAGG is used because its high average Z and density makes it compact and efficient. It is also non-radioactive, thus reducing random coincidence background. SiPMs are used because they are insensitive to magnetic fields from the MOT.

Two GAGG detectors are mounted at the positions shown in Figure 1b.

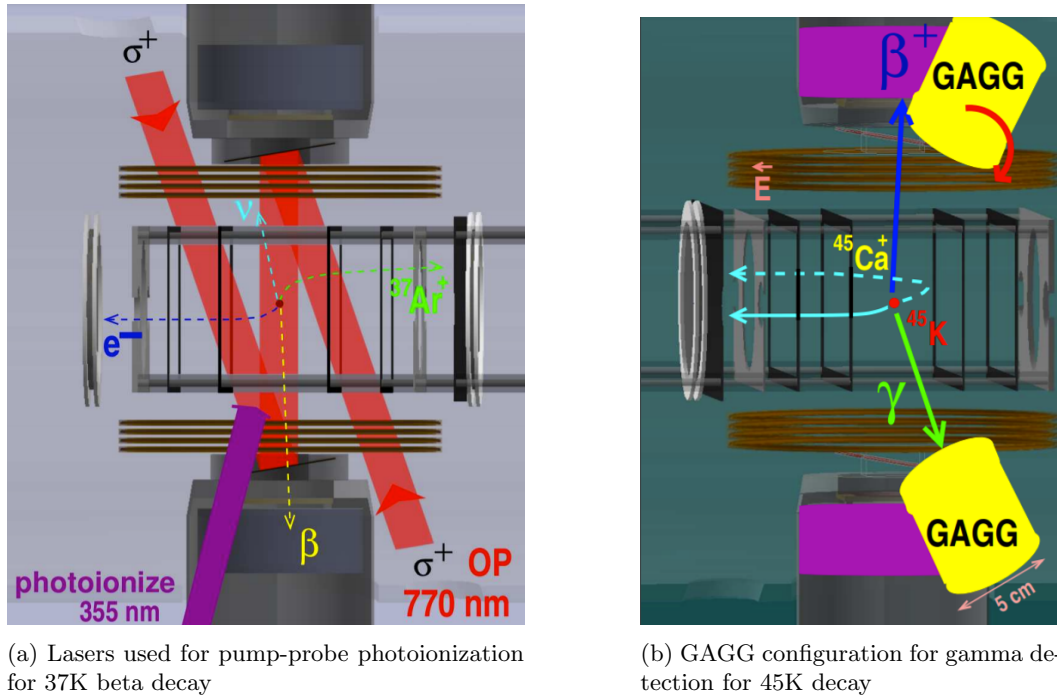


Figure 1: Experiment setup

## 2 355nm Laser and Fiber Coupling

The original setup includes a non-triggerable 355 nm laser, with light coupled into the cavity using cage optics mounted on one of the GAGG ports in Figure 1b. I attempted to replace the existing setup with Crylas' triggerable 355 nm laser, with fiber coupling into the cavity. The benefits of this updated setup include:

- Triggering allows for better control of the experiment
- The GAGG port becomes available for mounting the gamma detector
- The Crylas laser outputs higher power (35 mW)

Using fiber coupling provides the additional benefit of improved output beam mode quality.

The Crylas laser's specifications/manual are uploaded to TRINAT Documents, under /Home/Documents/Crylas documentation. The model number is Crylas FTSS355-Q2.

## 2.1 Beam Size/Shape

To verify the beam size and shape, a knife-edge measurement was used. As a knife-edge swept across the beam to block light, the transmitted power was measured using a photodetector connected to an oscilloscope. The experimental data was fitted to the expected transmitted power based on a Monte-Carlo simulation Monte-Carlo simulation. The resulting plot in Figure 2 indicates the MFD at the photodetector is 1676.40  $\mu\text{m}$ . Accounting for a divergence of 3.5 mrad (given by the Crylas spec sheet) and a  $44 \pm 5$  cm distance between the knife-edge and laser, the MFD at the beam waist is  $312.4 \pm 155.0$   $\mu\text{m}$ . This agrees within uncertainty with the spec sheet value of 242  $\mu\text{m}$ .

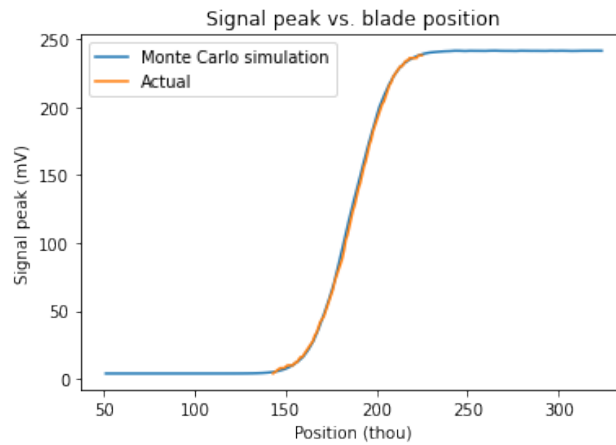


Figure 2: Measured vs simulated (Monte-Carlo) power transmitted in knife-edge measurement. This plot indicates a MFD of 1676.40  $\mu\text{m}$  at the measurement plane.

In addition, note that the experimental data in Figure 2 is not skewed (no unusual bumps or deviating shape aside from noise) relative to the simulated data. This qualitatively indicates that the beam is nearly Gaussian.

## 2.2 Fiber

### Challenges

At UV frequencies, the fiber is susceptible to additional damage mechanisms. Discoloration along the fiber can develop over time at low frequencies, which reduces transmission in a process known as solarization. In addition, many patch cords use epoxy to attach connector ends. Epoxy can burn when exposed to UV light, further reducing transmission. The fibers are especially susceptible to damage since the laser has relatively high peak power (3.5 kW).

Polarization-maintaining single-mode fiber must be used, as the mode-quality and polariza-

tion are important factors in this experiment. However, single-mode fibers typically have a smaller mode-field diameter (MFD), so the beam intensity is higher in single-mode fibers than in multi-mode fibers. This further increases the risk of damage from lasers with high peak powers.

Consider Thorlabs' typical single mode-fiber, which generally has MFD  $< 3 \text{ um}$ . The peak intensity is then

$$\frac{3.5 \text{ kW}}{\pi(3 \text{ um}/2)^2} = 0.495 \text{ GW/cm}^2$$

Scaling the  $1 \text{ GW/cm}^2$  laser-induced damage threshold (LIDT) for the Crylas laser's parameters the adjusted LIDT

$$1 \text{ GW/cm}^2 * \sqrt{\frac{(\text{pulse duration} = 1 \text{ ns})}{10 \text{ ns}}} * \sqrt{\frac{(\text{wavelength} = 355 \text{ nm})}{550 \text{ nm}}} = 0.254 \text{ GW/cm}^2$$

The peak intensity is nearly twice the LIDT so the risk of damage is high.

### **Selected Fiber**

To minimize damage, a custom patch cable was selected. The fiber is NKT Photonic's LMA-10-UV PM fiber, which is polarization-maintaining and single mode. This fiber has large mode area to reduce the peak intensity and is UV solarization resistant (the spec sheet is saved to TRINAT Documents under `Home/Documents/355 Crylas UV Laser`). The patch cable is assembled by Tratech Specialty Optical Fibers LLC with connectors optimized for UV applications.

## **2.3 Optical Assembly**

The optical assembly is shown in Figure 3. The collimator used is Thorlab's F810APC-405 package.

### **Power Reduction**

Between mirrors 1 and 2, a beam splitter, waveplate, and polarizer are used to turn down the beam's power. This allows one to minimize damage to the fiber during alignment, since high-power misaligned beams can cause damage to the endface (if the beam misses the fiber cavity) or cladding (if the beam's angle exceeds the fiber's numerical aperture).

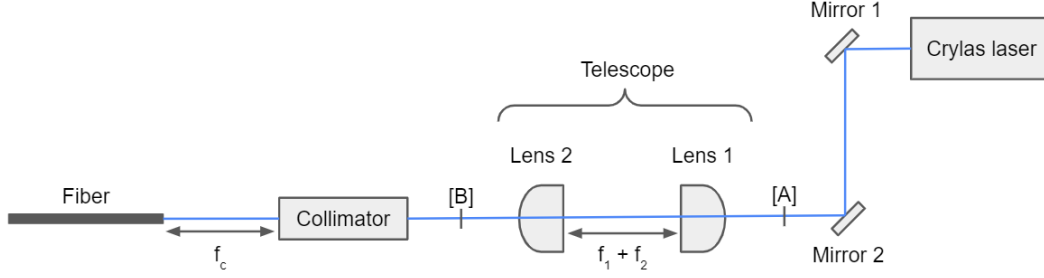


Figure 3: Layout for optical assembly.

### Telescope

The cage assembly includes a telescope, which can be used to adjust the beam size for optimal coupling. The beam should be no larger than the fiber's MFD to ensure its full power is transmitted. However, the smaller the beam area, the higher the intensity and probability of fiber damage. Therefore, the optimal beam MFD matches the fiber's MFD. One must also ensure the beam's divergence is within the fiber's numerical aperture (NA).

To calculate the desired magnification, the NKT fiber's MFD and NA at 355 nm was estimated as 8.0  $\mu\text{m}$  and 0.08. (These values are extrapolated based on the fiber's specification at other frequencies.) NA = 8.0  $\mu\text{m}$  corresponds with a half-angle divergence of 80 mrad. Since the collimator has  $f_c = 33.9$  mm, the desired beam size prior to collimation is

$$MFD + f_c * \tan(\text{divergence}) = 8.0 \text{ } \mu\text{m} + 33.9 \text{ mm} * \tan(80 \text{ mrad}) = 2.7 \text{ mm}$$

Accounting for the divergence of the Crylas laser (with beam waist radius  $w_0 = 121.0$   $\mu\text{m}$  and full-angle divergence = 3.10 mrad) along its  $\approx 400$  Mm path, the resulting beam size is

$$2 * 121 \text{ } \mu\text{m} + 400 \text{ mm} * \tan\left(\frac{3.1 \text{ mrad}}{2}\right) = 1.4 \text{ mm}$$

Therefore, the desired magnification is

$$M = \frac{2.7 \text{ mm}}{1.4 \text{ mm}} \approx 2$$

### Alignment

Two plane mirrors along the beam path are used to control the beam's angle and position. However, since these mirrors are quite far from the fiber, small changes in mirror angle produce large changes in position. In addition, the beam's position and angle are coupled,

which is a challenge since both parameters must be optimized for ideal fiber coupling. To decouple these parameters and provide small changes in position, the fiber collimator/mount has adjustable x-y position and angle.

## **Spatial Filtering**

Initially, the optical assembly included a pinhole at the focal point between the two lenses. Its intention was to clean up the beam by removing higher order modes, which could potentially damage the fiber.

This made alignment very challenging, since any adjustment of the beam's position/angle would misalign it from either the pinhole or the fiber. The pinhole was excluded from the final assembly to simplify the alignment process, since the original beam can be assumed to be nearly Gaussian based on Figure 2.

Single-mode fibers are generally expected to produce a cleaner beam than spatial filters, so there is no loss in the overall mode-quality by omitting the pinhole.

## **2.4 Procedure**

### **Alignment**

An iterative alignment process was most effective for coupling light into the fiber. During alignment, it is important to ensure the beam's power is minimized by the waveplate to prevent damage. If the Crylas laser is being used for alignment, ensure the collimator is blocked to prevent fiber exposure to misaligned beam. If the laser pointer is being transmitted backwards through the fiber, ensure the Crylas laser is blocked to prevent damage to the laser.

First, align the two mirrors using the 355 nm Crylas beam. Targets mounted on the cage optic can be used for alignment, and should have two alignment positions: Directly before the collimator (position [B] in Figure 3); and between the telescope and mirror 2 (position [A] in Figure 3). Iteratively align mirror 1 to hit the target at position [B], and mirror 2 to hit the target at position [A] until the beam runs parallel to the cage.

Next, use a laser pointer attached to the output end of the fiber to adjust the collimator/mount angle and position. This beam will propagate backwards through the assembly and the goal is to ensure it intersects with the forward propagating beam from the Crylas laser. The semi-translucence of a white sheet of paper allows one to see both beams simultaneously, so that one can check if the two beams overlap. Iteratively align the collimator's position by checking for intersection at position [B], and align the collimator's angle by

checking for intersection at position [A].

Finally, using only the backwards propagating laser pointer beam, adjust the telescope's length until the beam has constant size at all positions. If the laser pointer is not a 355 nm source, adjust the length depending on the expected focal shift.

## Transmission Optimization

After following the alignment procedure, the transmitted Crylas beam should be visible by eye. Slowly vary the telescope length, realigning the position and angle of the collimator until the transmitted beam is optimized. This can be done qualitatively by observation, or quantitatively using a photodetector and oscilloscope.

## 2.5 Results

### Tested Magnifications

As previously calculated, the desired magnification is  $M = 2$ . Using the available lens, magnifications of 1.67 ( $f_1 = 30$  mm,  $f_2 = 50$  mm) and 2.5 ( $f_1 = 20$  mm,  $f_2 = 50$  mm) were tested.

### Fiber Transmission

The transmission was maximized using the procedure described above. However, despite testing multiple magnifications, the maximum achievable transmission was 36.5%. Furthermore, over time transmission dropped to  $\approx 10\%$  despite realignment.

The transmission degradation implies the fiber is damaged over time. This is likely due to UV wavelengths (ie. potential solarization damage) or high power from the laser. Observation of the fiber end (on the side facing the incoming beam) revealed dark spots, which is another indicator of damage. It is unclear if the reduced transmission is due to these dark spots or a separate damage mechanism.

In order to prevent significant power losses, at least 50% fiber transmission was required for success. Since the fiber does not satisfy the transmission requirement and demonstrates degradation over time, single-mode fiber should not be used for 355 nm laser coupling.

The Crylas laser will continue to be used for the experiment, since it has high power and is triggerable. However, it will be coupled in free-space instead of using a fiber.

### 3 Gamma Detector

The original gamma detector is shown in Figure 4. The PTFE ensures diffuse reflection, and the ESR wrapping surrounding the PTFE increases reflectance. The optical gel is placed between the SiPM and the scintillator for optical coupling. This minimizes losses due to the high refractive index interface on the SiPM window and lower refractive index on the scintillator surface.

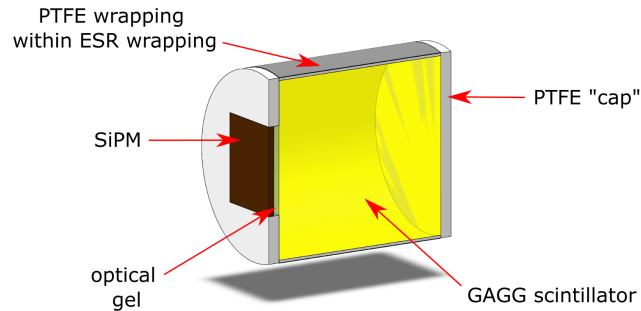


Figure 4: Detector assembly.

Note that additional research into the gamma detector is discussed in my previous presentation (saved to TRINAT documents under `/Home/Documents/Internal Reports/Co-op_Summary_Michelle_Khoo.pdf`). These findings include data on BGO vs. GAGG scintillator resolution; SiPM temperature sensitivity; and GEANT4 simulation results for different detector geometries.

#### 3.1 Bias Voltage Optimization

When biasing SiPMs, it is expected that increasing overvoltage yields a tradeoff between higher gain and photon detection efficiency (PDE), but higher dark current (ie. noise). To determine the optimal bias voltage, the overvoltage was varied between 3 V and 6 V. The plot in Figure 5 represents the FWHM of each peak in the Cs-137 and Co-60 spectrum as a function of overvoltage. The results indicate that energy resolution is consistent across overvoltages since there is no clear trend.

#### 3.2 Wrapping Sensitivity

Using GEANT4 simulations (saved to `trcomp` at `/home/trinat/mkhoo/code/GEANT4`) to model the detector according to Figure 4, the plot in Figure 6 was generated. This plot indicates  $\leq 5\%$  non-uniformity, which means the detector has relatively consistent light collection regardless of the position of the detected gamma (indicated by "Offset from detector

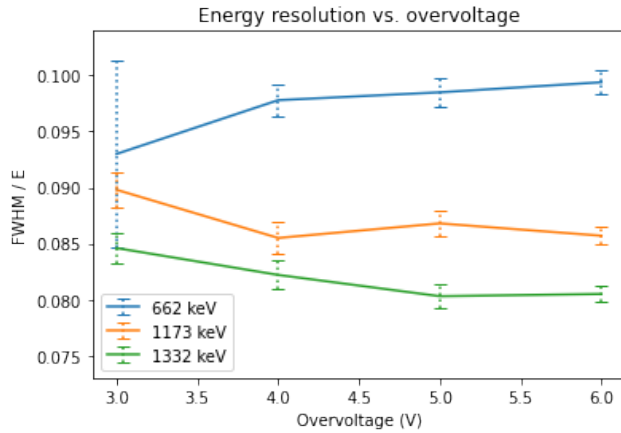


Figure 5: FWHM of Cs-137 and Co-60 peaks as a function of SiPM overvoltage.

center).

Notably, Figure 6 also indicates the detector is more sensitive to wrapping reflectance than expected. An increase from 93% to 98% reflectance corresponds with  $\approx 5\%$  more light collection. Since PTFE reflectance is thickness-dependent [2] and the current wrapping is  $<700$   $\mu\text{m}$  thick, we assume the reflectance is far less than Thorlab's quoted 93%. Thus there are major losses associated with the current detector. To reduce these losses and ensure  $\geq 98\%$  reflectance, ESR alone should be used to wrap the detector. Negligible losses are expected from the resulting specular reflection, since the GAGG crystal itself has a ground surface.

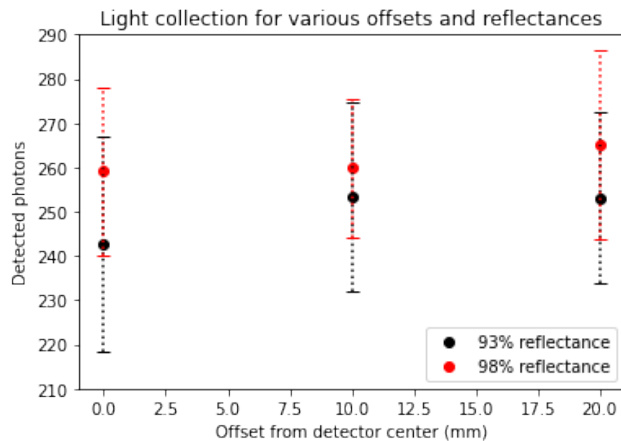


Figure 6: Detector efficiency as a function of wrapping reflectance and scintillation position.

### 3.3 Timing and Energy Signal Generation

#### Theory

By adding different discharge capacitors at the SiPM output, one can tradeoff between signal amplitude and timing. To optimize both energy and timing resolution, the summing circuit for the SiPM currents includes two outputs: A timing signal  $T_{sig}$  (fast response but smaller amplitude using a 1 nF capacitor) and an energy signal  $E_{sig}$  (slow response but large amplitude using a 100 nF capacitor). A simplified schematic is shown in Figure 7a and the expected signal based on SPICE simulations is shown in Figure 7b. From Figure 7b, one can see the timing signal has half the amplitude and half the rise time of the energy signal.

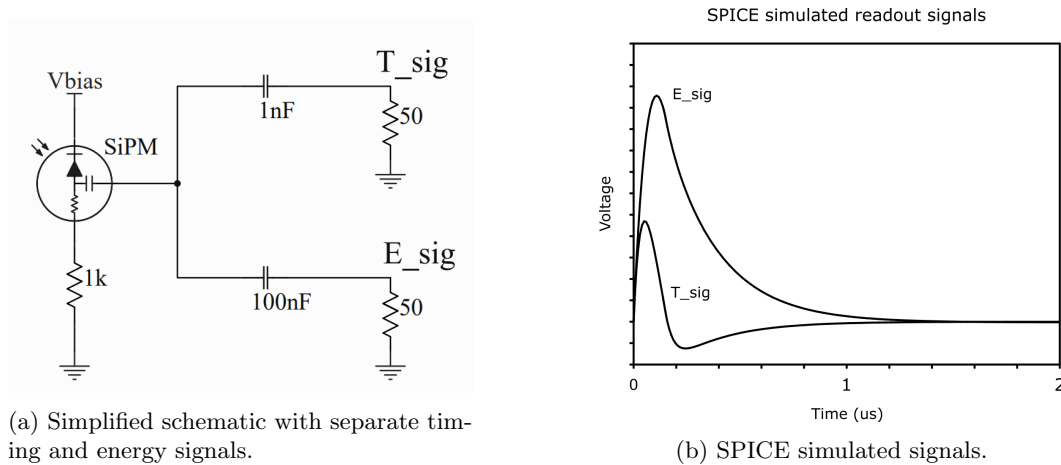


Figure 7: Separate timing and energy signals.

#### PCB Design

Separate energy and timing signals are implemented in the latest iteration of the SiPM summing circuit. The resulting PCB is an updated version of Tine Valencic's original prototype (outlined in his report in TRINAT Documents under `/Home/Documents/Internal Reports/Tine Valencic SURF report`) and uses the passive same summing configuration. The updated PCB has room for six (instead of the original four SiPMs per board) to be mounted, which allows for more light collection. Each PCB includes four timing outputs and four energy outputs, with MMCX connector outputs for each.

The Altium files for this PCB are saved to TRINAT Documents under `Home/Documents/Detectors/Gamma detector (GAGG)`. PDF/image versions of the schematic and layout are included in the Appendix for convenience.

### 3.4 Results

The GAGG detector was tested with the above recommendations implemented. The resulting modifications include:

- ESR (without PTFE) replaced the cylindrical PTFE wrapping and the cap with cutout (on the SiPM end) in Figure 4. Note that the PTFE cap without the cutout (opposite to the SiPM end) remains unmodified.
- The updated PCB is used for signal generation and current summing. This PCB includes timing and energy outputs, and uses six SiPMs (instead of four) for increased light collection.

#### Timing and Energy Signal

Raw timing (red) and energy (yellow) pulses are shown in Figure 8. As expected, the timing signal's rise time is approximately half the energy signal's rise time. However, the amplitude of the timing signal is much smaller than expected. This can be resolved using appropriate amplification.



Figure 8: Raw timing (red) and energy (yellow) signal pulses.

There is some overshoot in the energy signal, likely due to the discharging RC circuit in the PCB. If the negative overshoot is too large, the QDC can be damaged. To optimize this signal and minimize the overshoot, I recommend testing different capacitance values. The capacitors are SMD and can be swapped out (using a heat gun or careful soldering, and a pair of tweezers).

## Spectrum

The resulting spectrum (using the energy signal) is shown in Figure 9b. This spectrum is comparable with the original spectrum in Figure 9a, but the energy resolution appears to be slightly worse. This indicates that either the ESR wrapping or the updated PCB (perhaps due to overshoot in the energy signal) slightly decreases energy resolution.

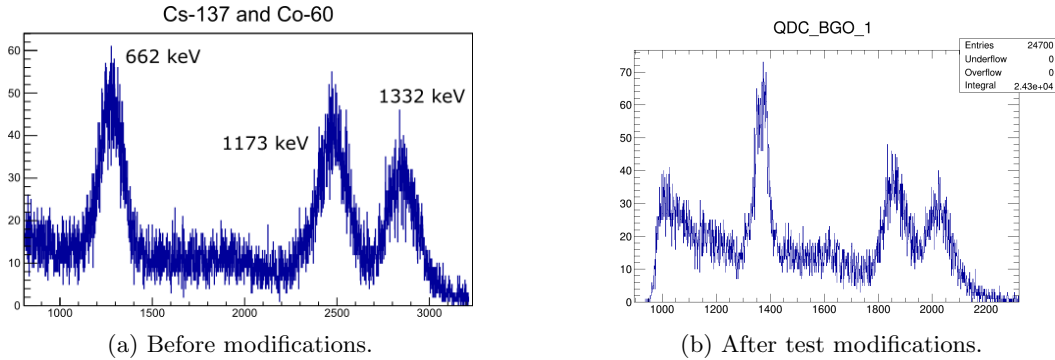


Figure 9: Cs-137 and Co-60 spectrum.

## Recommendations

As noted above, various capacitance values for the energy signal should be tested. This will allow one to minimize the overshoot and optimize the spectrum resolution.

In addition, it would be beneficial to attempt integration of the timing signal to TRINAT's overall gamma detection. This involves amplifying the timing signal; testing capacitance values to achieve a good trade-off between amplitude and rise time; and using the timing signal to trigger the QDC. One could then check if using separate timing and energy signals improves the timing data.

## 4 References

- [1] [https://www.thorlabs.com/newgrouppage9.cfm?objectgroup\\_id=3345#documentsPM-S350-HP](https://www.thorlabs.com/newgrouppage9.cfm?objectgroup_id=3345#documentsPM-S350-HP)
- [2] S. Ghosh et al., (2020), arXiv:2007.06626.

## Appendix

### Code

Scripts/simulations that may be helpful include:

- Physica code for fitting Cs-137, Co-60, and background spectra (saved to `trcomp` under `/mkhoo/code/GEANT4`)
- GEANT4 simulations (saved to `trcomp` under `/mkhoo/code/physica`)

### PCB Schematic and Layout

The front and back face of the PCB are shown in Figures 10 and 11. PDF versions of the Altium schematics are attached to the end of this report.

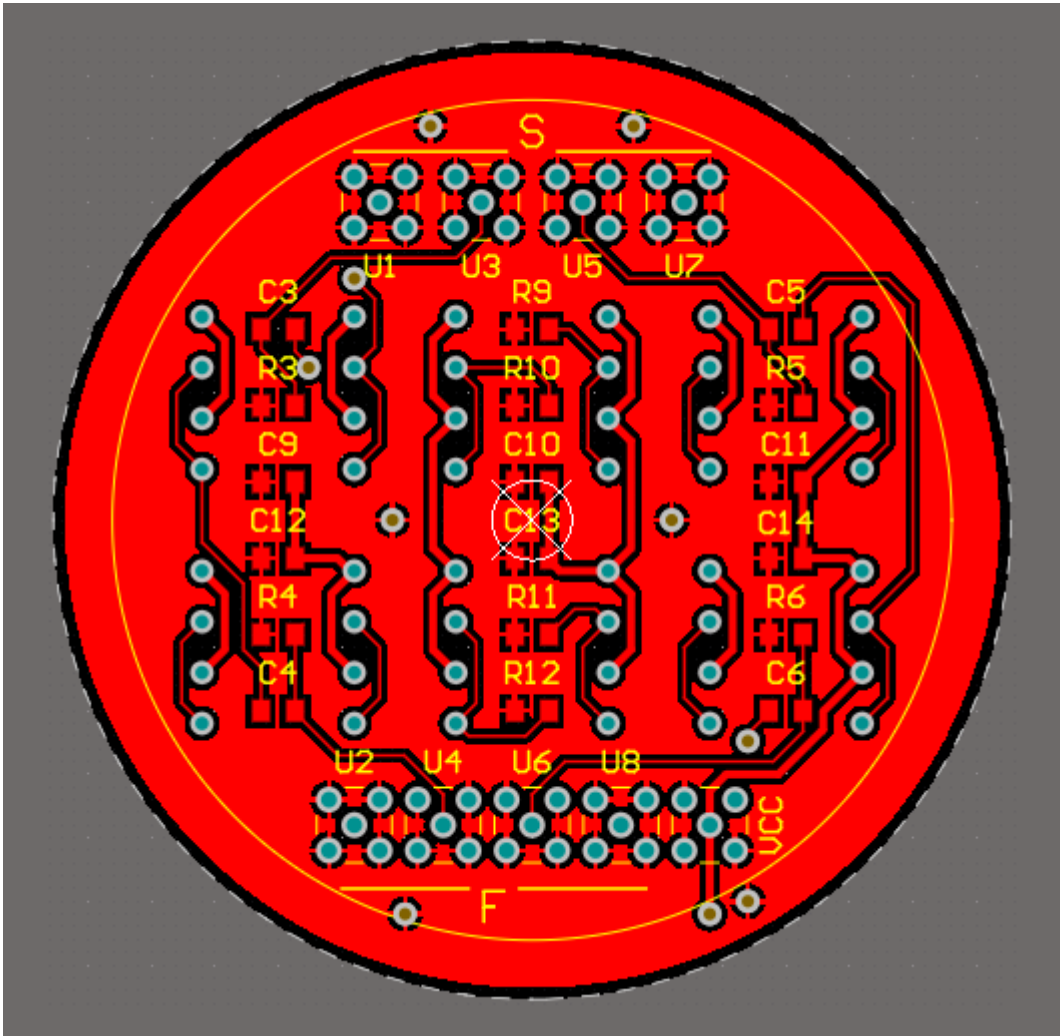


Figure 10: Front face of PCB.

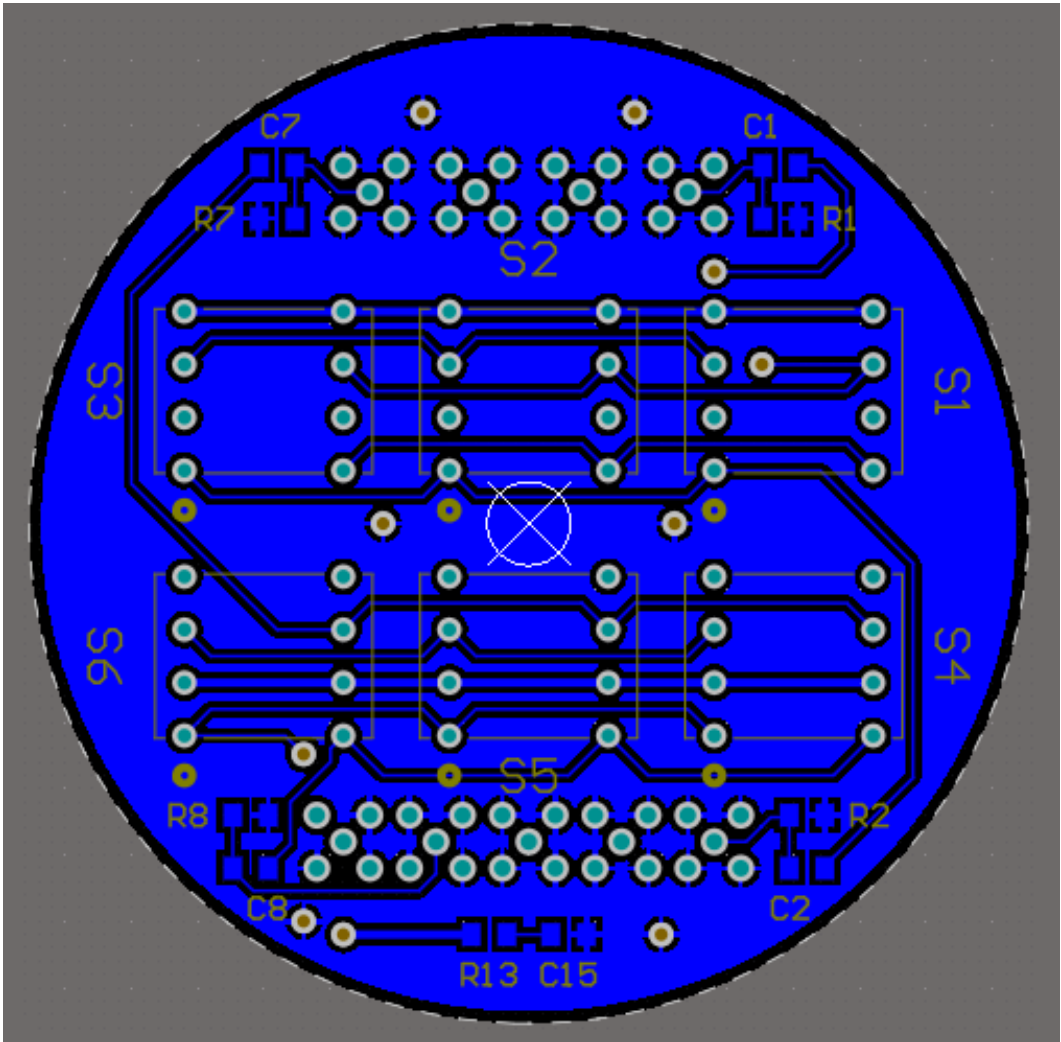


Figure 11: Back face of PCB.

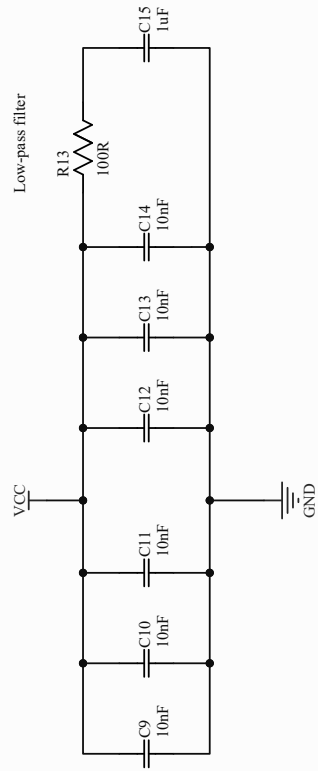


A

B

C

D



Title

Revision

Number

Size

A4

Sheet of

4

Drawn By:

C:\Users\...\PowerSchDec

Date:

5-01-2022

File:

C:\Users\...\PowerSchDec

A

B

C

D